Desalination and Water Treatment
www.deswater.com

doi: 10.5004/dwt.2017.21005

81 (2017) 223–232
June

Solar photocatalytic oxidation of an azo dye with immobilized $TiO_2/S_2O_8^{2-}$ in a component parabolic collector–reactor

Leila Ghalamchi, Mohammad Hossein Rasoulifard*, Mir Saeed Seyed Dorraji, Rahmat Pourata

Applied Chemistry Research Laboratory, Department of Chemistry, Faculty of Science, University of Zanjan, Zanjan, Iran, Tel. +982433052591; Fax: +982433052477; emails: m_h_rasoulifard@znu.ac.ir (M.H. Rasoulifard), ghalamchi_leila@yahoo.com (L. Ghalamchi), dorraji@znu.ac.ir (M.S.S. Dorraji), r_pourata@yahoo.com (R. Pourata)

Received 7 January 2017; Accepted 31 May 2017

ABSTRACT

Empirical modeling study of a new solar reactor for photocatalytic oxidation of wastewater containing toxic compounds is presented. The solar/$TiO_2/S_2O_8^{2-}$ treatment was mediated by a component parabolic collector (CPC) in functional condition (batch photoreactor). Field emission scanning electron microscopy analysis demonstrated favorable immobilization of TiO_2 on the outer surface of the glass tube, which was located in the focal path of CPC to measure the experimental reaction in enhancing the radiation intensity. A central composite design with a response surface methodology was applied to assess the relationships between operating variables and to evaluate the individual and main effects of several operating parameters (i.e., dye and persulfate concentration and reaction time) on treatment efficiency. In the best reaction conditions, 98.5% decolorization of DR23 was carried out with 21.1 mg L^{-1} of dye, 1.25 mM of $S_2O_8^{2-}$ in a reaction time of 90 min. Use of CPC photoreactor provides conditions for environmentally friendly wastewater treatment and enhances remarkable decolorization as compared with the commercial photocatalytic process under UV radiation which is mediated with persulfate.

Keywords: Advanced oxidation; Solar energy; Modeling; Nanoparticles; Photocatalysis

1. Introduction

Component parabolic collectors (CPCs) are motionless collectors with non-imaging optics that cause a surface to be reflective which can be designed for any given reactor shape. They collect all incident solar radiations within wide limits on a certain surface area and then reflect them toward the receiver that is placed in the focus [1]. The major advantage of CPCs is unchanging concentration factor for all values of sun zenith angle within the acceptance angle limit [2]. Therefore, this technological heightening can be used to design larger-scale systems to treat a greater volume of water for households or small communities.

Among the decontamination techniques, the solar advanced oxidation processes (AOPs) have received an increasing attention in the last decades [3–5]. Due to reproduction of free hydroxyl radicals ($HO^{\bullet}$), which are very reactive because of high oxidation potential, AOPs have been proven chiefly effective in the treatment of a range of wastewater containing recalcitrant organic pollutants [6]. Because they are capable of oxidizing and degrading almost any organic substance yielding CO_2 and inorganic ions as final products, they may be used as water treatment technologies to remove these contaminants [7,8].

Solar energy is free and has an important UVA component of around 3.5% of total irradiance [9]. The presence of concentrating devices gives several times the energy per area unit that naturally sun does, but they do not allow the reactor to use diffuse radiation (visible and UV).

Among conventional AOPs, the heterogeneous photocatalysis sub-method with solar/TiO_2, illuminated by light energy higher than their band gap energy states of electron

* Corresponding author.

and hole pair (e^-/h^+), have attracted attention for their ability in the detoxification of wastewater [10]. Because it is highly reactive, non-toxic relatively economical and chemically stable, technological interest in TiO_2 (E_g = 3.2 eV) has focused on its photocatalytic and hydrophilic characteristics [11,12]. The use of solar light was found to be an economic option compared with artificial UV radiation [13,14]. Although TiO_2 is widely used in suspension (slurry) with excellent performance, it requires expensive filtration to separate the catalyst from the treated water, by using different types of mutants, such as glass [15,16], polymer [17,18] and ceramics [19,20]. However, the selection of an adequate supporter for water applications is not an issue.

The efficiency of solar photoactivated treatments may be enhanced by the use of solar CPC reactors. Their high efficiency in solar radiation (both direct and diffuse) collection accelerates the inactivation rates of the different solar treatments because of the optimal collection of solar UVA photons [21,22]. The present study is a step forward in comparing the heterogeneous (TiO_2) photocatalytic degradation of the Direct Red 23 azo dye (DR23) under sunlight. The study's main objective is to analyze the feasibility of the decolorization and mineralization of DR23 by solar/TiO_2/$S_2O_8^{2-}$ processes. The different operational parameters (time, DR23 and $S_2O_8^{2-}$ concentration) that affect the efficiency of heterogeneous photocatalysis processes during the oxidation of DR23 were studied. Borosilicate glass was employed as a supporter because of the semiconductor's excellent adherence to it, and its transparency is in the range of TiO_2 activity (~300–400 nm) [23]. The reaction was carried out in a solar CPC. The intensity of the sunlight was enhanced when the solar CPC reactor was applied.

2. Materials and methods

2.1. Material

The Direct Red 23 azo dye (color index) was provided by Alvan Sabet Co. (Iran) and used as received without further purification. The UV–Vis absorption spectra and molecular structure of DR23 are illustrated in Table 1. The chemical used in the experiments, TiO_2-P25 (Degussa, Germany) $K_2S_2O_8$ (Merck, Germany) were of reagent grade.

2.2. Design and build of solar pilot plant

The CPC was designed and built to consist of two coaxial tubes (29 cm × 3.2 cm ID), of which the outer tube made of quartz and the borosilicate tube (29 cm × 15 mm ID) was placed at the focal path of the reflector. The parabola reflector was built of steel. The total collector surface was 750 cm^2 (concentration factor[1] = 2.59) and the illuminated volume was 100 mL. The CPC reactor was held in a fixed platform with an inclination degree of approximately 39° (corresponding to the local latitude) and north–south orientation on the flat roof at the University of Zanjan in Iran. The schematic of CPC was shown in Fig. 1.

2.3. Immobilization of TiO_2-P25 on outer surface of glass tube

To prepare the immobilized TiO_2-P25 on outer surface of the glass tube (1.5 cm diamond × 29 cm length), the heat attachment method was applied [24,25]. A suspension of commercial Degussa P25 TiO_2 was prepared in 30 mL ethanol with pH adjusted to about 4 [26] which was then sonicated in an ultrasonic bath (T/460 H, Windaus) under the frequency of 60 Hz (170 W). Next, 30 mL of suspension was carefully poured on the outer surface of the borosilicate tube and allowed to dry at 70°C for 2 h. After drying, the tube was heated to 480°C, kept for 3 h, and then cooled to room temperature by immediately showering with tap water, and then sequentially washing several times with deionized water for the removal of weakly attached TiO_2-P25 particles (Fig. 2). Throughout the heating process and because of the reaction between OH groups from the catalyst surface and the support, one molecule of water was lost and one oxygen bridge was created. Therefore, the adherence of the catalyst to the support was enhanced [27]. Before the deposition, the tube surface was scrubbed mechanically with a tungsten carbide stone and treated using a dilute acid solution of HF and then washed in a solution of NaOH (0.01 M) in order to increase the number of OH groups [28,29]. Field emission scanning electron microscopy (FESEM) was carried out using a Mira microscope (Mira3, Tescan, Kohoutovice, Czech Republic) to evaluate the surface morphology of nano-TiO_2.

2.4. Methods

All solar photocatalytic experiments were carried out under similar conditions on sunny summer days (July and August) under clear sky between 11 a.m. and 3 p.m. when the highest irradiation was present (Table 2). All the solutions were prepared by dissolving the requisite quantity of dye in distilled water. The pH of the solution was adjusted using H_2SO_4 and NaOH solutions. All experiments were performed in a CPC solar reactor with a capacity of 1,500 mL. According to

1. The ratio reflective surface to received surface.

Table 1
Characteristics of DR23

DR23 properties		
Name	C.I. Direct Red 23	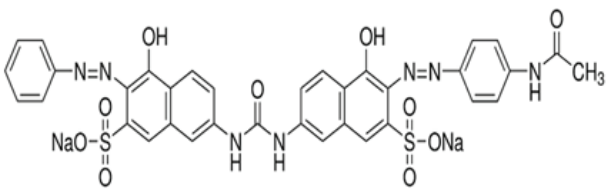
Type	Dianionic	
Azo group	Two	
λ_{max}	507 nm	
Molecular formula	$C_{35}H_{25}N_7Na_2O_{10}S_2$	
Molecular weight (g mol^{-1})	813.72	
Color index number	29160	

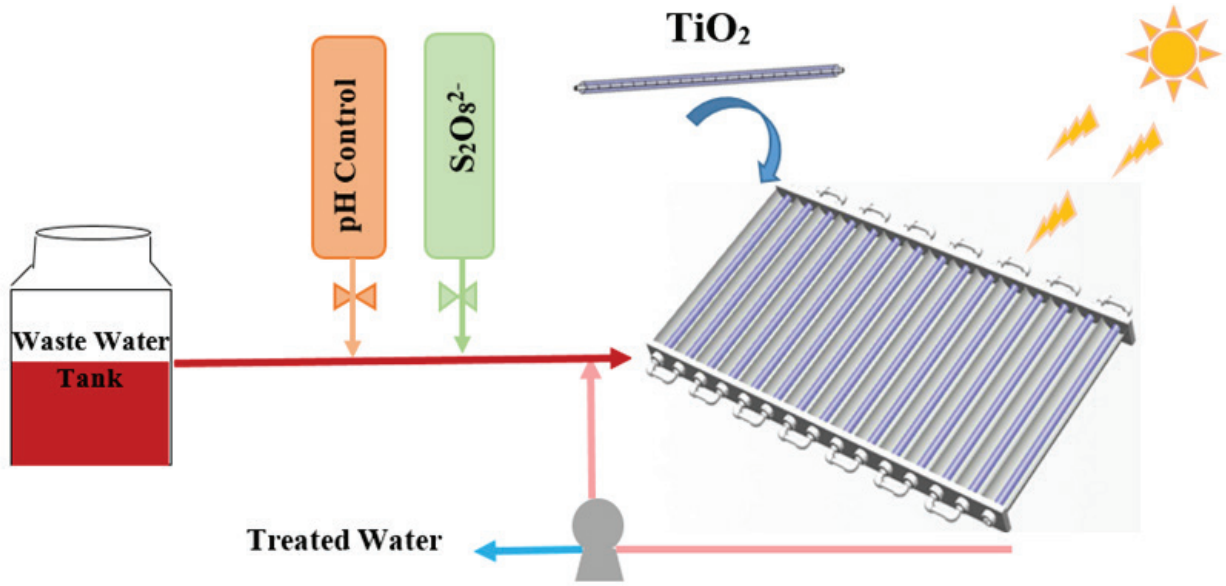

Fig. 1. Schematic of component parabolic collector.

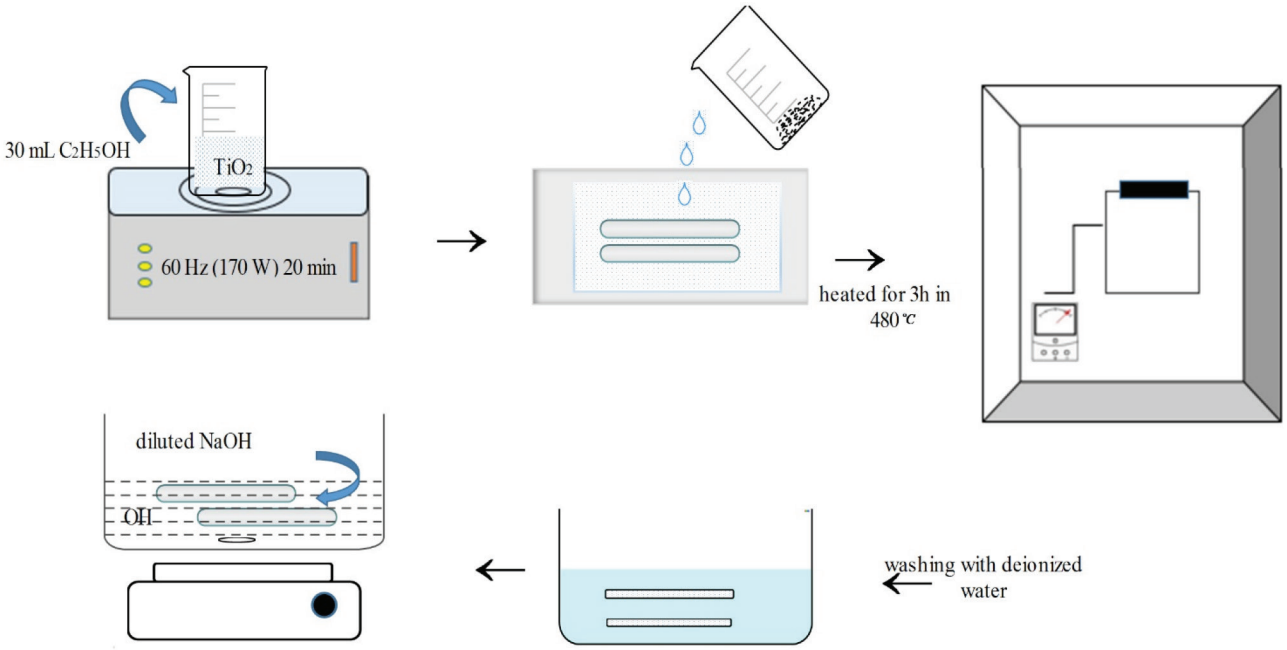

Fig. 2. Schematic of the heat attachment method for immobilization of TiO_2.

the designed experimental, the specified amount of $S_2O_8^{2-}$ was added to the dye solution. After mixing, the solution pumped to CPC solar collector. The flow rate was 190 mL min^{-1} and circulated to the solar reactor. The absorbance of the sample solution containing DR23 was monitored at 507 nm, using a spectrophotometer (Model UV-160, Shimadzu Co., Japan).

2.5. Experimental design

To find the optimum conditions for the degradation of the DR23 dye in the CPC reactor, the experimental design as a function of the selected main factors has to be determined. This rotatable experimental plan was carried out as a central composite design (CCD) consisting of 20 experiments. For three variable ($n = 3$) and two levels (low (–) and high (+)), the total number of experiments were 20, as determined by the following expression: 2^n ($2^3 = 8$ factor points) + $2n$ ($2 \times 3 = 6$: axial points) + 6 (central points: six replications), as shown in Tables 3 and 4, for solar/TiO_2/$S_2O_8^{2-}$. The factors (variables) in these experiments were the dye concentration (X_1), $S_2O_8^{2-}$ concentration (X_2) and time (X_3).

A regression model was applied, and the findings were analyzed using Minitab version 16 (Minitab Institute, USA). The response (Y) was related to the selected variables

Table 2
Weather conditions for selected days for experiments

Date	Minimum temperature (°C)	Mean temperature (°C)	Maximum temperature (°C)	UV index
2016/07/06	14	24	34	8
2016/07/15	14	24	35	8
2016/07/22	17	24	31	8
2016/07/26	16	24	31	8
2016/08/3	17	24	31	8
2016/08/07	16	24	32	8
2016/08/12	14	24	33	8
2016/08/15	17	24	31	8
2016/08/20	17	24	32	8
2016/08/21	15	23	31	8

Table 3
The original and uncoded levels of the input variables

Parameter	Levels				
	–2	–1	0	+1	+2
(X_1) Dye	15	22.5	30	37.5	45
(X_2) $S_2O_8^{2-}$	0.05	0.35	0.65	0.95	1.25
(X_3) Time	10	30	50	70	90

Table 4
CCD, experimental plan and results

Std order	Run order	Dye (mg L^{-1})	$S_2O_8^{2-}$ (mM)	Time (min)	Decolorization (%)	
					(Exp.[a])	(Pred.[b])
15	1	30	0.65	50	36.00	36.22
17	2	30	0.65	50	37.00	36.22
2	3	37.5	0.35	30	10.10	10.68
7	4	22.5	0.95	70	72.40	71.06
20	5	30	0.65	50	35.60	36.22
19	6	30	0.65	50	37.00	36.22
6	7	37.5	0.35	70	20.72	21.14
16	8	30	0.65	50	35.00	36.22
4	9	37.5	0.95	30	26.58	26.25
13	10	30	0.65	10	21.20	21.82
1	11	22.5	0.35	30	32.00	30.93
12	12	30	1.25	50	50.00	50.89
9	13	15	0.65	50	61.50	63.13
11	14	30	0.05	50	16.96	16.82
5	15	22.5	0.35	70	53.00	52.57
8	16	37.5	0.95	70	42.00	42.31
14	17	30	0.65	90	59.40	59.53
18	18	30	0.65	50	36.00	36.22
10	19	45	0.65	50	15.00	14.13
3	20	22.5	0.95	30	45.00	43.82

[a]Experimental.
[b]Predicted.

according to the full second-order polynomial (quadratic) model. According to uncoded variables, the second-order model can be expressed as follows:

$$Y = \beta_0 + \beta_1 X_1 + \beta_2 X_2 + \beta_3 X_3 + \beta_{11} X_1^2 + \beta_{22} X_2^2 + \beta_{33} X_3^2 + \beta_{12} X_1 X_2 + \beta_{12} X_1 X_3 + \beta_{23} X_2 X_3 \quad (1)$$

where β_0, β_j (j = 1, 2 and 3), β_{jj} (j = 1, 2 and 3) and β_{ij} (i = 1, 2 and 3; $i < j$) are intercepted, linear, quadratic and interaction regression coefficients, respectively. Based on the proposed model, the analysis of variance (ANOVA) was applied to determine the interaction between the response and process variables. The coefficient of determination (R^2) was applied to define the quality of fit for the polynomial model, and the statistical significant was checked according to the F value (Fischer variation ratio) and p value (significant level). Finally, in order to visualize the individual and the interaction effects of the independent variables on the photocatalytic degradation of DR23 in the immobilized-TiO_2 based on PC under solar light, two-dimensional contour plots, which are three-dimensional response surface plots, were drawn.

3. Results and discussion

3.1. Characterization of nano-TiO_2 immobilized and recycle test of immobilized TiO_2 on the glass tube

Fig. 3 shows FESEM images of nano-TiO_2 immobilized on the outer surface of the glass. As shown, the scrubbed tube has a porous structure with a surface area suitable to use as support for the immobilization of nano-TiO_2. As shown in Figs. 3(a) and (b), the immobilization of nano-TiO_2 was favorably stabilized on the glasstube at four different resolutions, which led to complete coverage.

To investigate the durability of immobilized TiO_2 after a long period of operation, the TiO_2 was immobilized after the six operations and compared with the new immobilized TiO_2. Fig. 4 illustrates that the photocatalytic activity of TiO_2 on the glass tube did not decrease significantly after the sixth operation. This proves that immobilized TiO_2 is not deactivated during reactions and can be used again. The percentage of dye removal after six periods of experiments during 90 min of irradiation was 93% and there was a negligible difference with the first test. Operational conditions were 25 mg L^{-1} of dye and 1.25 mM of $S_2O_8^{2-}$.

3.2. Model fitting and statistical analysis

A central composite experimental design with six axial points ($\alpha = 2$) and six replications at the center point, requiring a total of 20 experiments, should be considered in response surface modeling. The predicted values for color removal efficiencies and experimental results are shown in Table 4. Considering these results, an empirical relationship between the response and independent variables was achieved and is expressed by the following second-order polynomial Eq. (2):

$$Y = 42.43 - 1.53X_1 + 16.33X_2 + 0.60X_3 + 0.01X_1^2 - 6.58X_2^2 + 0.002X_3^2 + 0.298X_1X_2 - 0.018X_1X_3 + 0.23X_2X_3 \quad (2)$$

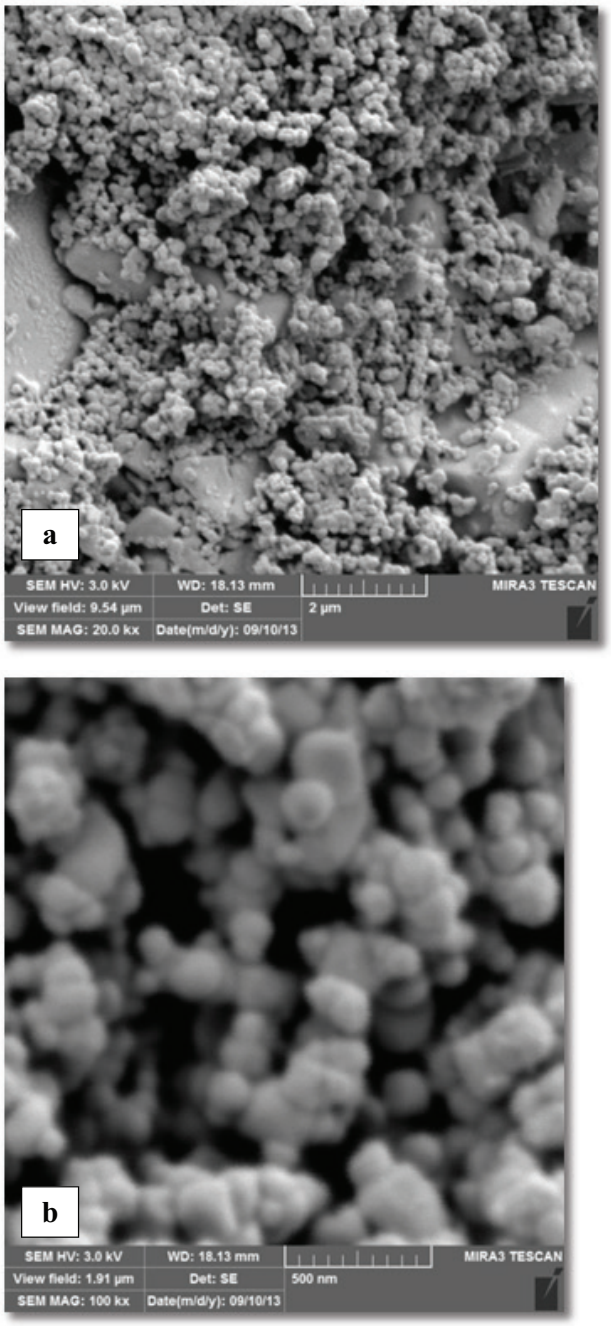

Fig. 3. FESEM images of nano-TiO_2 immobilized on outer surface of glass tube in different magnification: (a) 20,000 and (b) 100,000.

Table 5 illustrates that the results of the quadratic response surface model fit the ANOVA. ANOVA is used to test the significance and the adequacy of the model. The results showed that the regression model had a high value of coefficient of determination (R^2 = 0.997). The R^2 value showed the amount of variation that could be explained by the experimental factors and their interactions.

99.7% of the variations in dye removal efficiency can be explained by the independent variables signifying that the model also explains about 5% of the variation. Table 6 shows the corresponding values and the parameter estimate. The evaluation of each coefficient, which is essential for realizing the pattern of mutual interactions between the test variable was showed by the probability value (p value). A p value less than 0.05 at 95% confidence level indicated that the model terms were significant. According to Table 6, the corresponding coefficient will be more noticeable if the Fischer's value (F test) of the quadratic model is higher than the related critical value for degree of freedoms equal to 9 and 10 at the significant level of 0.05 ($F_{crtical,0.05,9,10}$ = 2.04) [30,31].

Fig. 5 presents the comparison between the calculated and experimental values of the response variable of decolorization efficiency (Table 4), by using the results of the second-order polynomial equation (Eq. (2)). The correlation coefficient for this plot is 0.997. The results showed that the experimental values were in good agreement with the predicted values.

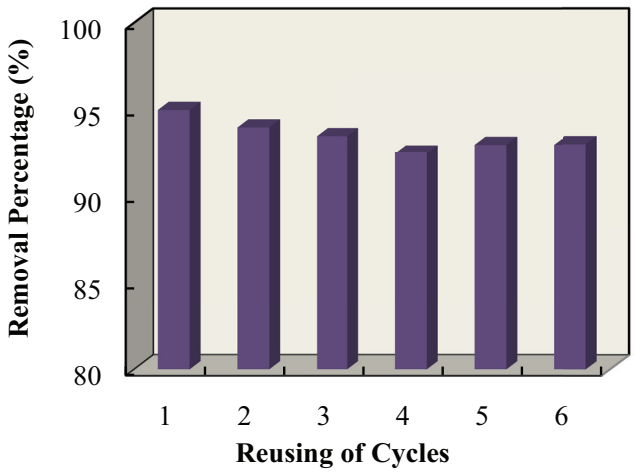

Fig. 4. Reusability behavior of immobilized TiO_2 in the solar/TiO_2/$S_2O_8^{2-}$ process for decolorization of 20 mg L^{-1} DR23 solution in the presence of 1.0 mM $S_2O_8^{2-}$ and 90 min.

Table 5
ANOVA for fit of decolorization efficiency from CCD

Source of variation	SSs	DOF	Adj. SS	Adj. MS	F value	p value
Regression	5,121.25	9	5,121.25	569.028	436.27	0.000
Residual total	13.04	10	13.04	2.060		
Total	5,134.29	19				
Lack of fit	9.94	5	9.94	1.989	3.21	0.113

Note: R^2 = 99.75%; $R^2_{(adj)}$ = 99.52%.
DOF, degree of freedom; SS, sum of square; MS, mean square.

Table 6
Factor effects and associated *p* values and *T* values

Term		Coefficient	*p* Value	*T* value
Constant	β_0	42.43	0.000	5.799
Dye	β_1	–1.53	0.000	–5.058
$S_2O_8^{2-}$	β_2	16.33	0.047	2.264
Time	β_3	0.60	0.000	5.509
Dye × dye	β_{11}	0.01	0.025	2.636
$S_2O_8^{2-} \times S_2O_8^{2-}$	β_{22}	–6.58	0.027	–2.599
Time × time	β_{33}	0.002	0.001	4.886
Dye × $S_2O_8^{2-}$	β_{12}	0.298	0.128	1.659
Dye × time	β_{13}	–0.018	0.000	–6.922
$S_2O_8^{2-}$ × time	β_{23}	0.23	0.006	3.467

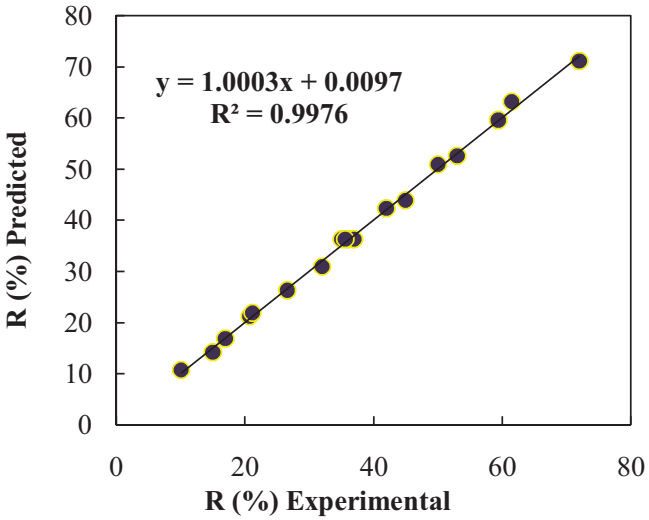

Fig. 5. Comparison of the experimental results of decolorization efficiency with those calculated via CCD results equation.

3.3. Effect of parameters for removal of DR23

The response surface and contour plots of the model's predicted responses, with two constant variables and the others varying within the experimental ranges, were obtained applying Minitab software. Response surface plots provide a way to predict the dye removal efficiency for various values of the examined variables and the type of interactions between these variables was identified by the contours of the plots [32].

Each Cantor curve with consideration of an infinite number of combinations of the two tested parameter, while the other were constant at their respective zero level. The circular contour of response surfaces showed that the interaction between the corresponding variables was insignificant. On the opposite, an elliptical or saddle shape of the contour plots indicated that the interaction between the corresponding variables was remarkable [33,34]. The results showed that the response surface plots successfully predicted the decolorization efficiency of different values of the tested variables, and the contours of the plots helped to detect the type of interactions among these variables [35].

As shown in Fig. 6, the response surface and contour plots were developed as a function of reaction time and initial dye concentration, while the initial $S_2O_8^{2-}$ concentration was kept constant at 0.65 mM, which was the central level. As shown in Fig. 6, color removal efficiency increased with the increasing reaction time in all applied initial dye concentrations. On the other hand, decolorization efficiency decreased with the increase in initial dye concentration. A higher concentration increased the number of dye molecules, except $HO^{\bullet}$ and $SO_4^{-\bullet}$ radical concentration, so the removal rate diminished. In addition, high color of dye concentration causes the penetration of photons from solar light into the dye solution, thereby decreasing the concentration of hydroxyl and sulfate radicals [35]. The found results were in agreement with the literature reporting that increases in the initial concentration of pollutants decreases treatment efficiency [36–39].

Fig. 6 illustrates the response surface and contour plots of decolorization efficiency as a function of reaction time and initial $S_2O_8^{2-}$ concentration. It is clear that decolorization efficiency increased with an increase in the amount of $S_2O_8^{2-}$. As an electron scavenger, persulfate promotes the formation of sulfate radicals, which accelerate the removal of dye. Because an increase in persulfate concentration leads to a decrease in the removal time, we concluded that persulfate plays an important role in the photocatalytic system. An increase in the concentration of persulfate indicates that additional sulfate radicals will be generated by photolysis, photoactivation or by the electrons in the conduction band. In the process of photocatalytic degradation, $S_2O_8^{2-}$ has a dual role. It gets a photogenerated electron from the conduction band and thus promotes the charge separation and it also forms $HO^{\bullet}$ and $SO_4^{-\bullet}$ radicals via superoxide, according to Eqs. (3)–(6). The possible reaction of $S_2O_8^{2-}$ with the photogenerated intermediates cannot be excluded [40]:

$$S_2O_8^{2-} + e_{CB} \rightarrow SO_4^{2-} + SO4^{-\bullet} \quad (3)$$

$$SO_4^{\bullet-} + H_2O \rightarrow HSO_4^- + OH^{\bullet} \quad (4)$$

$$S_2O_8^{2-} + h\upsilon \rightarrow 2SO_4^{\bullet-} \quad (5)$$

$$2SO_4^{-\bullet} + H_2O \rightarrow HSO_4^- + HO^{\bullet} \quad (6)$$

In addition to the effect of each of the variables, such as dye and $S_2O_8^{2-}$ concentration and time of reaction on the removal of dye individually, it is important to check the effects of the interaction of these variables, especially the two-factor interaction effect. Interaction plots were constructed by plotting both variables on the same graph, as shown in Fig. 7. The chart shows that the persulfate and DR23 concentration critically affected the rate of the dye degradation, but the interaction between them was not remarkable because contour plots formed parallel lines. Furthermore, as the figure shows, there was no interaction between the time and the dye, and time and persulfate, based on the lack of intersecting lines.

3.4. Determination of optimal conditions for the decolorization of DR23

The desired goal of decolorization efficiency was defined as "maximum" to achieve the highest treatment performance. The optimum values of the process variables for the maximum decolorization efficiency are shown in Table 7. The predicted values were verified by a further experimental test. The results indicated that the maximal decolorization efficiency was obtained when the values of each parameter were set as the optimal values, which was in good agreement with the values predicted by the model. These results imply that in this study, the strategy used to optimize the decolorization conditions and to obtain the maximal decolorization

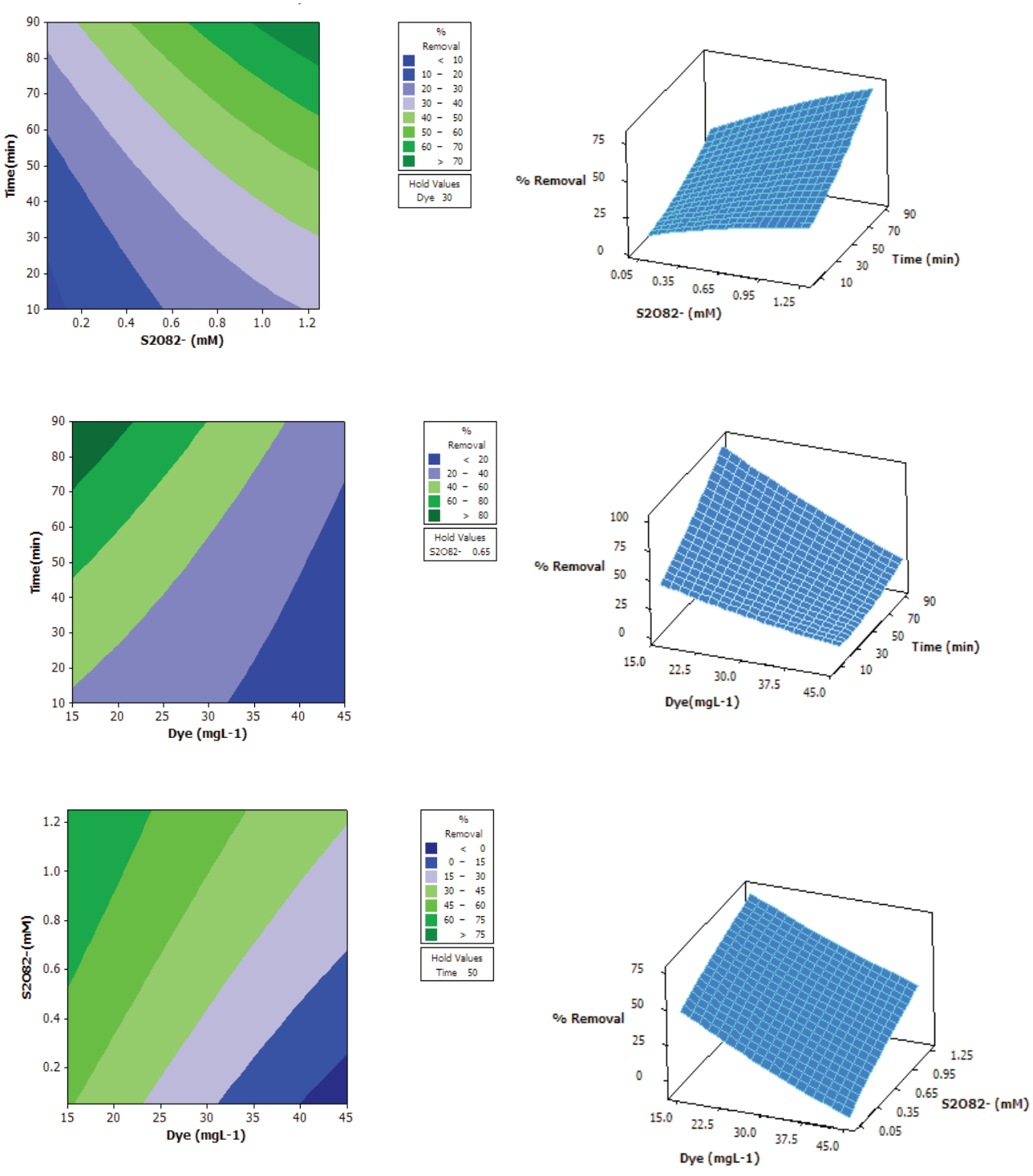

Fig. 6. The response surface plot and contour plot of the decolorization efficiency (*R*%) as a function of parameters.

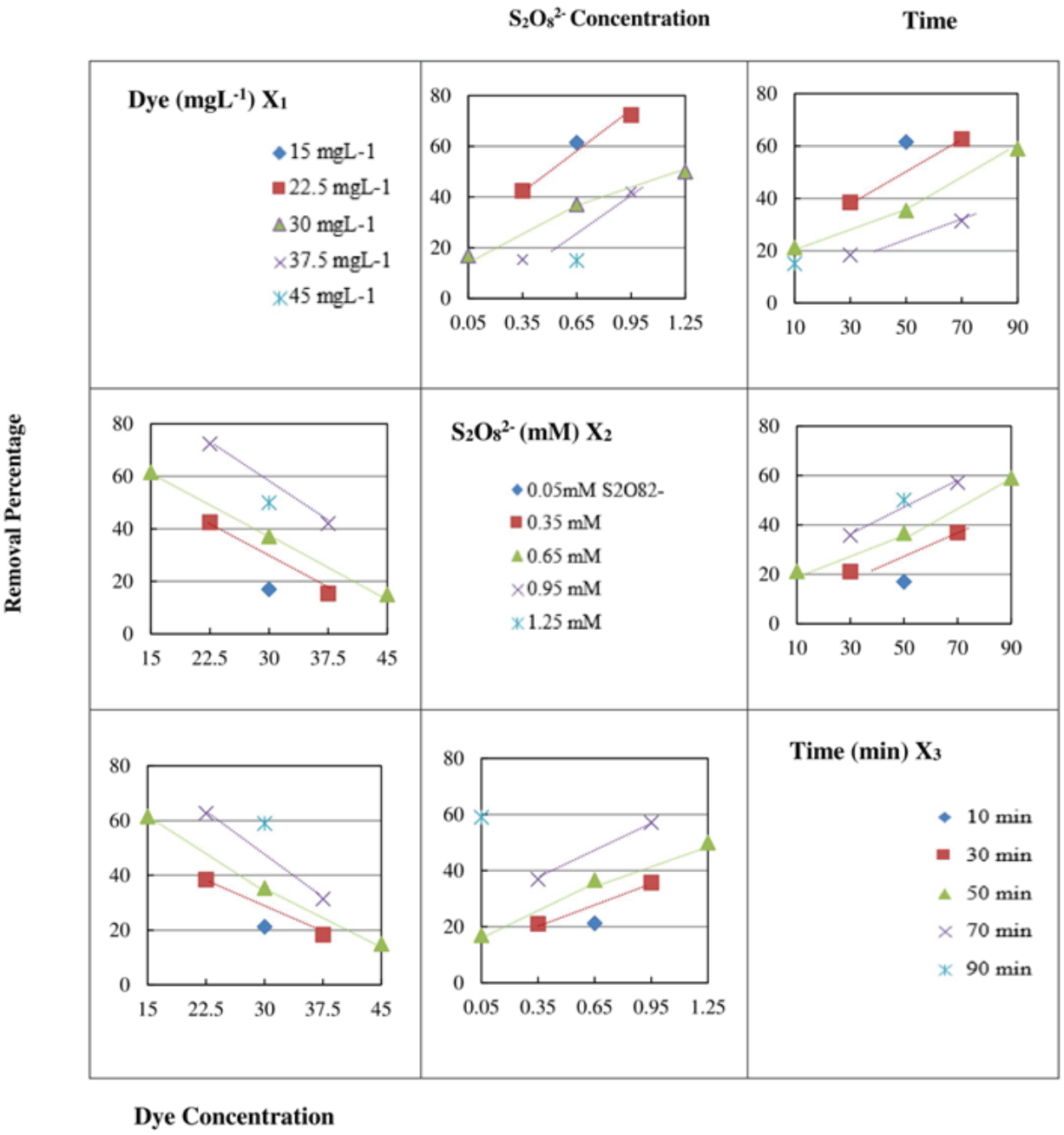

Fig. 7. Two-way interaction plots for color removal (%) in uncoded values.

Table 7
Comparison of experimental and predicted values of removal of DR23 at the optimal levels predicted by RSM

Optimal conditions		Predicted value (%)	Observed value (%)	UV–Vis absorption spectrum
(X_1) Dye	21.1 mg L^{-1}	100	98.5	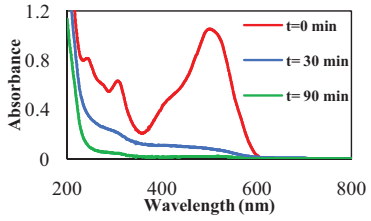
(X_2) $S_2O_8^{2-}$	1.25 mM			
(X_3) Time	90			

efficiency by response surface methodology (RSM) for the decolorization of DR23 by solar/TiO_2/$S_2O_8^{2-}$ processes was successful. Moreover, time-dependent UV–Vis spectrum of DR23 solution during irradiation was showed in Table 7. The absorption peaks, corresponding to the dye, weakened and finally disappeared under reaction, which indicated that the dye had been removed. The spectrum of DR23 in the visible region exhibited a main band with the maximum at 507 nm. The decrease in absorption peaks of DR23 at λ_{max} = 507 nm shown in this figure indicated the rapid degradation of azo dye. This result also indicates that the nitrogen-to-nitrogen double bond (–N=N–) of the azo dye was the most active site for oxidative attack. The complete discoloration of the dye was observed after 90 min in the optimized conditions.

4. Conclusion

This study showed that heterogeneous photocatalysis (solar/TiO_2) of DR23 had the best performance at 98.5% decolorization. The obtained results in this study suggested that the solar/TiO_2/$S_2O_8^{2-}$ process in the CPC has potential for polishing conventionally treated. Because their characteristics render this system a potential candidate for a quick and inexpensive water treatment technology. In addition, the quadratic model expressed a functional relationship between the degradation efficiency of DR23 and three independent variables: initial dye concentration, $S_2O_8^{2-}$ dosage and reaction time. A satisfactory goodness-of-fit was observed between the predicted and the experimental results, which reflected the applicability of RSM in optimizing the process used in the simulated dyestuff effluent decolorization. Significantly, enhanced performance was observed under higher $S_2O_8^{2-}$ dosage and lower dye concentration.

Acknowledgment

The authors thank the University of Zanjan, Iran, for financial and other supports.

Conflict of Interest

The authors declare that they have no conflict of interest.

References

[1] S.A. Kalogirou, Solar thermal collectors and applications, Prog. Energy Combust. Sci., 30 (2004) 231–295.
[2] M.A. Sousa, C. Gonçalves, V.J.P. Vilar, R.A.R. Boaventura, M.F Alpendurada, Suspended TiO_2-assisted photocatalytic degradation of emerging contaminants in a municipal WWTP effluent using a solar pilot plant with CPCs, Chem. Eng. J., 198–199 (2012) 301–309.
[3] P.Y. Chan, M.G. El-Din, J.R. Bolton, A solar-driven UV/chlorine advanced oxidation process, Water Res., 46 (2012) 5672–5682.
[4] B.S. Souza, F.C. Moreira, M.W. Dezotti, V.J. Vilar, R.A. Boaventura, Application of biological oxidation and solar driven advanced oxidation processes to remediation of winery wastewater, Catal. Today, 209 (2013) 201–208.
[5] M.H. Rasoulifard, M. Fazli, M.R. Eskandarian, Performance of the light-emitting-diodes in a continuous photoreactor for degradation of Direct Red 23 using UV-LED/$S_2O_8^{2-}$ process, J. Ind. Eng. Chem. Res., 24 (2015) 121–126.
[6] L. Gomathi Devi, S. Girish Kumar, K. Mohan Reddy, C. Munikrishnappa, Photo degradation of Methyl Orange an azo dye by advanced Fenton process using zero valet metallic iron: influence of various reaction parameters and its degradation mechanism, J. Hazard. Mater., 164 (2009) 459–467.
[7] K. Ikehata, M.G. El-Din, Aqueous pesticide degradation by hydrogen peroxide/ultraviolet irradiation and Fenton-type advanced oxidation processes: a review, J. Environ. Eng. Sci., 5 (2006) 81–135.
[8] B. Nakonechny, N. Graham, Y. Zhang, M. Nakonechny, Degradation of endocrine disrupting chemicals by ozone/AOPs, Ozone Sci. Eng., 29 (2007) 153–176.
[9] A. Speltini, M. Sturini, F. Maraschi, D. Dondi, G. Fisogni, E. Annovazzi, A. Buttafava, Evaluation of UV-A and solar light photocatalytic hydrogen gas evolution from olive mill wastewater, Int. J. Hydrogen Energy, 40 (2015) 4303–4310.
[10] S. Malato, P. Fernandez-Ibanez, M.I. Maldonado, J. Blanc, W. Gernjak, Decontamination and disinfection of water by solar photocatalysis: recent overview and trends, Catal. Today, 147 (2009) 1–59.
[11] A. Fujishima, T.N. Rao, D.A. Tryk, Titanium dioxide photocatalysis, J. Photochem. Photobiol., C, 1 (2000) 1–21.
[12] M.R. Hoffmann, S.T. Martin, W. Choi, D.W. Bahnemann, Environmental applications of semiconductor photocatalysis, Chem. Rev., 95 (1995) 69–96.
[13] A. Safarizadeh-Amiri, J.R. Bolton, S.R. Cater, Ferrioxalate-mediated solar degradation of organic contaminants in water, Solar Energy, 56 (1996) 439–443.
[14] R. Bauer, G. Waldner, H. Fallman, S. Hager, M. Klare, T. Krutzler, S. Malato, P. Maletzky, The photo-Fenton reaction and the TiO_2/UV process for wastewater treatment – novel developments, Catal. Today, 53 (1999) 131–134.
[15] M. Karches, M. Morstein, P. Rudolf von Rohr, R.L. Pozzo, J.L. Giombi, M.A. Baltanas, Plasma-CVD-coated glass beads as photocatalyst for water decontamination, Catal. Today, 72 (2002) 267–279.
[16] G. Balasubramaninan, D.D. Dionysiou, M.T. Sudian, I. Baudin, J.M. Lâiné, Evaluating the activities of immobilized TiO_2 powder films for the photocatalytic degradation of organic contaminants in water, Appl. Catal., B, 47 (2004) 73–84.
[17] T. Kemmitt, N.I. Al-Salim, M. Waterland, V.J. Kennedy, A. Markwitz, Photocatalytic titania coatings, Curr. Appl. Phys., 4 (2004) 189–199.
[18] B. Sánchez, J.M. Coronado, R. Candal, R. Portela, I. Tejedor, M.A. Anderson, D. Tompkins, T. Lee, Preparation of TiO_2 coatings on PET monoliths for the photocatalytic elimination of trichloroethylene in the gas phase, Appl. Catal., B., 66 (2006) 295–301.
[19] P. Zhang, J. Tian, R. Xu, G. Ma, Hydrophilicity, photocatalytic activity and stability of tetraethyl orthosilicate modified TiO_2 film on glazed ceramic surface, Appl. Surf. Sci., 266 (2013) 141–147.
[20] T.L.R. Hewer, S. Suárez, J.M. Coronado, R. Portela, P. Avila, B. Sanchez, Hybrid photocatalysts for the degradation of trichloroethylene in air, Catal. Today, 143 (2009) 302–308.
[21] C. Navntoft, E. Ubomba-Jaswa, K. McGuigan, P. Fernandez-Ibáñez, Effectiveness of solar disinfection using batch reactors with non-imaging aluminium reflectors under real conditions: natural well-water and solar light, J. Photochem. Photobiol., B., 93 (2008) 155–163.
[22] O.A. McLoughlin, P.F. Ibáñez, W. Gernjak, S.M. Rodríguez, L.W. Gill, Photocatalytic disinfection of water using low cost compound parabolic collectors, Solar Energy, 77 (2004) 625–633.
[23] R. Portela, B. Sánchez, J.M. Coronado, R. Caudal, S. Suárez, Selection of TiO_2-support: UV-transparent alternatives and long-term use limitations for H_2S removal, Catal. Today, 129 (2007) 223–230.
[24] S. Sakthivel, M.V. Shankar, M. Palanichamy, B. Arabindoo, V. Murugesan, Photocatalytic decomposition of leather dye: comparative study of TiO_2 supported on alumina and glass beads, J. Photochem. Photobiol., A., 148 (2002) 153–159.
[25] M.A. Behnajady, N. Modirshahla, M. Mirzamohammady, B. Vahid, B. Behnajady, Increasing photoactivity of titanium dioxide immobilized on glass plate with optimization of heat attachment method parameters, J. Hazard. Mater., 160 (2008) 508–513.

[26] C. Hachem, F. Bocquillon, O. Zahraa, M. Bouchy, Decolourization of textile industry wastewater by the photocatalytic degradation process, Dyes Pigm., 49 (2001) 117–125.
[27] M. Faisal, M. Abu Tariq, M. Muneer, Photocatalysed degradation of two selected dyes in UV-irradiated aqueous suspensions of titania, Dyes Pigm., 72 (2007) 233–239.
[28] A.R. Khataee, M.N. Pons, O. Zahraa, Photocatalytic degradation of three azo dyes using immobilized TiO_2 nanoparticles on glass plates activated by UV light irradiation: influence of dye molecular structure, J. Hazard. Mater., 168 (2009) 451–457.
[29] I.H. Cho, K.D. Zho, Photocatalytic degradation of azo dye (Reactive Red 120) in TiO_2/UV system: optimization and modeling using a response surface methodology (RSM) based on the central composite design, Dyes Pigm., 75 (2007) 533–543.
[30] A.R. Khataee, V. Vatanpour, M. Rastegar, Remediation of the textile dye brilliant blue from contaminated water by Fenton-like process: influence of aromatic additives, Turk. J. Eng. Environ. Sci., 32 (2008) 367–376.
[31] M.B. Kasiri, H. Aleboyeh, A. Aleboyeh, Modeling and optimization of heterogeneous photo-Fenton process with response surface methodology and artificial neural networks, Environ. Sci. Technol., 42 (2008) 7970–7975.
[32] Y. Li, C. Chang, T. Wen, Application of statistical experimental strategies to H_2O_2 production on Au/graphite in alkaline solution, Ind. Eng. Chem. Res., 35 (1996) 4767–4771.
[33] A.R. Khataee, M. Fathinia, S. Aber, M. Zarei, Optimization of photocatalytic treatment of dye solution on supported TiO_2 nanoparticles by central composite design: intermediates identification, J. Hazard. Mater., 181 (2010) 886–897.
[34] H.L. Liu, Y.R. Chiou, Optimal decolorization efficiency of Reactive Red 239 by UV/TiO_2 photocatalytic process coupled with response surface methodology, Chem. Eng. J., 112 (2005) 173–179.
[35] M.A. Rauf, N. Marzouki, B.K. Körbahti, Photolytic decolorization of Rose Bengal by UV/H_2O_2 and data optimization using response surface method, J. Hazard. Mater., 159 (2008) 602–609.
[36] J. Feng, X. Hu, P.L. Yue, H.Y. Zhu, G.Q. Lu, Discoloration and mineralization of Reactive Red HE-3B by heterogeneous photo-Fenton reaction, Water Res., 37 (2003) 3776–3784.
[37] N. Daneshvar, S. Aber, V. Vatanpour, M.H. Rasoulifard, Electro-Fenton treatment of dye solution containing Orange II: influence of operational parameters, J. Electroanal. Chem., 615 (2008) 165–174.
[38] D. Salari, A. Niaei, S. Aber, M.H. Rasoulifard, The photooxidative destruction of C.I. Basic Yellow 2 using UV/$S_2O_8^{2-}$ process in a rectangular continuous photoreactor, J. Hazard. Mater., 166 (2009) 61–66.
[39] N. Daneshvar, M.H. Rasoulifard, A.R. Khataee, F. Hosseinzadeh, Removal of C.I. Acid Orange 7 from aqueous solution by UV irradiation in the presence of ZnO nano powder, J. Hazard. Mater., 143 (2007) 95–101.
[40] C.H. Wu, Photodegradation of C.I. Reactive Red 2 in UV/TiO_2-based systems: effects of ultrasound irradiation, J. Hazard. Mater., 167 (2009) 434–439.